Journal of The Electrochemical Society, **157** (12) H1095-H1100 (2010)
0013-4651/2010/157(12)/H1095/6/$28.00 © The Electrochemical Society

Interfacial Charge Distribution-Dependent Modulation of Luminescence Characteristics of InGaN/GaN Multiquantum-Barrier Heterosystems

Jen-Cheng Wang,[a] Chia-Hui Fang,[a] Hui-Tang Shen,[a] Ya-Fen Wu,[b] and Tzer-En Nee[a,z]

[a]*Department of Electronic Engineering, Chang Gung University, Tao-Yuan 333, Taiwan*
[b]*Department of Electronic Engineering, Ming Chi University of Technology, Taipei 243, Taiwan*

We have investigated the unique correlations between the excitonic characteristics and the interfacial charge distribution of InGaN/GaN multiple quantum well (MQW) light-emitting diodes (LEDs) over a broad range of temperatures. From the intensity–current–voltage characteristics of InGaN/GaN MQW LEDs, we observed a remarkable reduction and modulation in the distribution of the leakage charge over the light-emitting layer when adopting the multiquantum-barrier (MQB) structure. For nonunity ideality factors, which we extracted from current–voltage analyses, we found that it was the temperature that determined the carrier transport mechanism in the heterodevices. Furthermore, carrier tunneling processes, determined from the extent of charge accumulation, led to more-anomalous values of the pseudotemperature (T_0) and characteristic energy (E_0), which resulted from an abnormal deterioration of the luminescence intensities for a low effective density of states (DOS). We found that low-indium-content MQB devices exhibited inherently low values of T_0 over a broad range of temperatures. These values were associated with a low characteristic energy, a low charge population of the multilayer interface states, and a more-effective DOS. The signal intensity in the temperature-dependent electroluminescence spectrum deteriorated considerably at temperatures below 180 K, consistent with the presence of a greater number of charges at a higher value of E_0.
 [DOI: 10.1149/1.3494146]

Manuscript submitted April 7, 2010; revised manuscript received July 11, 2010. Published October 14, 2010.

Several recent attempts have been made to improve the structural and optoelectrical characteristics of nitride-based optoelectronic devices, which have many potential applications because of their thermal stability and high luminescence efficiency.[1] Gallium nitride-based semiconductors are used in a variety of high-power and high-temperature devices because of their wide band gaps, high chemical stability, and relatively high saturation drift velocities.[2,3] High-quality InGaN-based multiple quantum well (MQW) heterostructures are being investigated widely because of their potential applications in light-emitting diodes (LEDs) and laser diodes that can be operated at wavelengths from the visible to the ultraviolet. The presence of piezoelectric polarization, spontaneous polarization, and spinodal decomposition in wurtzite epitaxial heterolayers grown incoherently on (0001)-oriented sapphire substrates leads to nitride materials and devices exhibiting inherently abnormal electronic and optical properties.[4-8] Nevertheless, in nanoscale crystalline structures, epitaxial heterosystems can feature misfit dislocations, which can lead to nonradiative recombination and decreased emission efficiency.

Several technologies and applications have been developed to advance the performance and reliability of light-emitting devices. If we are to improve device performance even further, it will be essential that we understand the effects of these defects on the carrier injection mechanisms and excitonic recombination processes. Although striking technological advances have been made, carrier (electron and hole) transport and radiative processes in InGaN structures remain poorly understood. For example, when the excess carriers overflow from the active layer to the cladding layer in epitaxial InGaN-based heterosystems featuring misfit dislocations in their nanocrystalline structures, the presence of defects and nonradiative recombination centers critically affects the performance of such devices; understanding the unique spectral responses requires the ability to examine electronic transport behavior within heterodevices. On the other hand, studies of the internal quantum efficiency of carrier transport in the recombination zone have revealed a remarkable reduction in the degree of leakage of electrons and holes over the light-emitting layer when adopting a multiquantum-barrier (MQB) structure.[9-11]

High ideality factors exist in nitride-based p–n junction diodes at temperatures below 300 K.[12] Schubert et al. recently modeled the current–voltage (I–V) characteristics of diodes fabricated from a bulk GaN p–n junction and a p–n junction structure featuring a p-type AlGaN/GaN superlattice.[12] They found that the externally measured ideality factor of a p–n junction diode is the sum of the ideality factors of the individual rectifying junctions within the diode. On the other hand, taking into account the surface-state energy distributions of the interfaces, Levine proposed[13] an alternative approach toward examining the departure of the ideality factor from unity, where a temperature-independent parameter T_0—the so-called pseudotemperature—and the characteristic energy E_0—obtained from I–V measurements at various temperatures—can be used to determine the mechanism of injected current transport. In this study, we investigated the unique correlations existing between the electrical and optical characteristics of InGaN/GaN MQW LEDs featuring MQBs by examining the evolution of the ideality factors over the temperature range from 20 to 300 K. We found that the carrier transport process was essentially responsible for the improvement in the luminescence characteristics.

Experiments

The samples investigated in this study were prepared through metallorganic vapor phase epitaxy on c-plane sapphire substrates. Ammonia (NH_3), trimethylgallium (TMG), trimethylindium (TMI), silane (SiH_4), and bis(cyclopentadienyl)magnesium (Cp_2Mg) were used as either precursors or dopants. The layer structure for the conventional sample consisted of a 20-nm-thick GaN buffer layer, a 3-μm-thick Si-doped n-type GaN layer, an undoped GaN layer featuring five periods of $In_{0.15}Ga_{0.85}N$/GaN MQWs, and a 100-nm-thick Mg-doped p-type GaN layer. The doping concentrations, calibrated using Hall measurements, were nominally 3×10^{18} and 5×10^{17} cm^{-3} for the Si-doped n-type GaN layer and the Mg-doped p-type GaN layer, respectively. The thicknesses of the InGaN wells and the GaN barriers in the MQW structures were 2 and 11 nm, respectively. The structures of the other samples were similar but with different types of five-period $In_xGa_{1-x}N$/GaN MQBs in the active regions of these devices. The total thicknesses of the MQB structures were fixed at 11 nm; they consisted of a 1-nm-thick $In_xGa_{1-x}N$ well layer and a 1-nm-thick GaN barrier layer for each period of the $In_xGa_{1-x}N$/GaN MQB structure. For comparison, barriers were also prepared having three different In compositions, i.e., five-period $In_xGa_{1-x}N$/GaN in the active regions of these

[z] E-mail: neete@mail.cgu.edu.tw

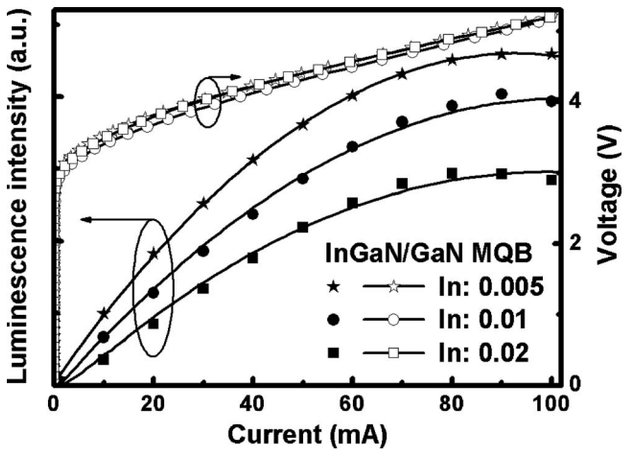

Figure 1. *L–I–V* characteristics, under direct current operation, of InGaN/GaN LEDs incorporating MQBs of various compositions.

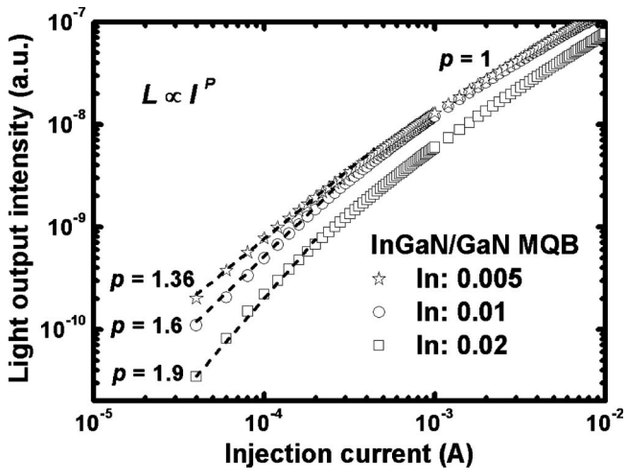

Figure 2. Dependence of light output on the injection current for LEDs incorporating MQBs featuring In contents (x) of 0.005, 0.01, and 0.02, respectively.

two devices having values of x for the low-, medium-, and high-In-content $In_xGa_{1-x}N$/GaN MQB samples of 0.005, 0.01, and 0.02, respectively. The InN molar compositions for the MQW and MQB structures were both examined through photoluminescence and X-ray diffraction (XRD) measurements (not shown here). High-resolution XRD measurements were performed using a Bede D1 system to study the epilayer properties of the MQWs and MQBs. For the $In_xGa_{1-x}N$/GaN MQB samples featuring low (x = 0.005), medium (x = 0.01), and high (x = 0.02) In contents, the measured X-ray diffraction linewidths were 200, 245, and 270 arcsec, respectively. Thus, the X-ray diffraction linewidths broadened upon increasing the In content in the barriers; this observation indicates that crystalline randomization, intermixing, and/or interfacial roughness existed in the InGaN/GaN nanostructures.[11,14] The LED chips were fabricated over a broad area (350×350 μm^2) using standard photolithography processes. Ti/Al/Ti/Au and Ni–Au, which were deposited through electron beam evaporation, were employed for the n- and p-type electrodes, respectively. After deposition, thermal alloying was performed using a rapid thermal processor in a furnace to improve the ohmic properties of both electrodes. The current–voltage (I–V) characteristics of the experimental LEDs were measured using an HP-4156C semiconductor parameter analyzer; the output powers of the LEDs without the encapsulated epoxy were measured using a calibrated integrating sphere at room temperature. For temperature-dependent I–V measurements, all of the MQW LEDs possessing MQB chips were mounted on the Cu cold stage of a variable-temperature closed-cycle He cryostat that allowed the temperature to be varied over a wide range (from 300 to 20 K); they were then excited using a Keithley 2430 instrument. For electroluminescence (EL) measurements, the samples were mounted in a closed-cycle He cryostat and excited by a current of 20 mA over a broad temperature range. The luminescence signal was dispersed through a 0.5-m monochromator and then it was detected by a Si photodiode while employing a standard lock-in amplification technique.

Results and Discussion

The room-temperature output intensity–current–voltage (L–I–V) characteristics of all of the samples (Fig. 1) reveal that the output intensity was linear at moderate injection currents, indicating a dominant radiative recombination and constant quantum efficiency.[14] When the current was increased further, the light output reached saturation, possibly caused by a heating effect of the higher injection current. The reverse currents at −4 V of the low-, medium-, and high-In-content $In_xGa_{1-x}N$/GaN MQB samples and the sample having merely a GaN barrier were 4×10^{-10}, 1×10^{-9}, 4×10^{-9}, and 3×10^{-8} A, respectively, at 300 K. Here, the leakage current was much higher than the classical diffusion and generation/recombination current, which should be small in magnitude in wide-bandgap materials.[15] We attribute this high reverse current to defect-assisted tunneling, band-to-band tunneling, or leakage of electrons and holes. Therefore, as the excess carriers overflow from the active layer to the cladding layer, defects and nonradiative recombination centers might critically affect the performance of these devices. Our results indicate that an MQB structure can significantly suppress carrier leakage and enhance carrier confinement. From a study of the internal quantum efficiency in the recombination zone, we observed a remarkable reduction in the degree of leakage of electrons and holes over the light-emitting layer when adopting the MQB structure. On the other hand, we found that the maximum output intensity decreased upon increasing the In composition of the InGaN/GaN MQB. We attribute this behavior to the greater distribution and modulation of interface states and the less-effective density of states (DOS), which resulted in excess carrier overflow to the GaN barriers where they either recombined radiatively or became extinguished nonradiatively after being trapped by defects.

Figure 2 displays the room-temperature light output intensity–current (L–I) characteristics of the LEDs incorporating MQBs. The light output L varies with respect to I^p, where p is a power factor reflecting the effect of deep-level states on the recombination process,[15] within a specific injection regime. The superlinear dependence of L on I ($p > 1$) at low current densities results from dominant nonradiative tunneling processes; i.e., carriers tunnel into (i) the available deep-lying defect states in the space-charge region followed by nonradiative recombination or (ii) the MQWs and recombine nonradiatively via bandgap states. For low injection currents, the parameter p decreased from 1.9 to 1.36 upon decreasing the In composition as a result of suppression of nonradiative tunneling processes in the space-charge regions. Under moderate injection conditions, the diffusion/recombination mechanism dominated; i.e., the parameter p approached unity. Another feature in Fig. 2 that reveals the influence of the defects on light emission is the current level at which the nonradiative deep-level states were saturated. Nevertheless, epitaxial InGaN-based heterosystems display misfit dislocations, which would lead to nonradiative recombination and decreased emission efficiency, in their nanocrystalline structures. This result suggests that the well-known high-density defects in III–V nitrides heteroepitaxially grown on sapphire are, in general,

optically inactive. Our results reveal both the inhibition of nonradiative recombination and the enhancement of localization effects when adopting the MQB structure.

To examine the electronic transport behavior in heterodevices, we observed that the experimental temperature dependence of the *I–V* characteristics was contingent on the carrier dynamical mechanisms in the InGaN/GaN heterosystems possessing InGaN/GaN barriers. In general, the Shockley equation gives the expected theoretical *I–V* relationship of a p–n junction. To describe the experimentally measured characteristics, we used the following equation:[16]

$$I = I_s\left[\exp\left(\frac{eV}{nkT}\right) - 1\right] \quad [1]$$

where I_s is the reverse saturation current, e is the electronic charge, k is Boltzmann's constant, and T is the thermodynamic temperature. The so-called "ideality factor," n, of the diode takes a value of 1 for a diffusion current flowing across the junction and a value of 2 when the recombination current dominates.[16] Values of n as high as 7.0 have been found, however, for InGaN/GaN diodes; high ideality factors appear for nitride-based p–n junction diodes when the temperature is below 300 K.[12] Shah et al.[12] proposed that GaN-based LEDs can be modeled as a series of rectifying unipolar heterojunctions and metal–semiconductor junctions, each having an associated ideality factor. From modeling of the *I–V* characteristics,[17] Zhu et al. found recently that the externally measured ideality factor of a p–n junction diode is the sum of the ideality factors of the individual rectifying junctions within the diode. This dependence reveals that the ideality factors of the individual rectifying junctions add up to the total device ideality factor when considering the p–n junction of the diode, a nonohmic metal–semiconductor junction, or any other rectifying junction. The Sah–Noyce–Shockley theory[18] suggests that the forward current in a p–n junction is dominated by recombination of minority carriers injected into the neutral regions of the junction and recombination of carriers in the space-charge region. Both of these recombination mechanisms are strongly voltage-dependent. For voltage-dependent carrier recombination processes, the dependence of the ideality factors (extracted from the *I–V* analysis) on temperature and voltage will determine the carrier transport mechanisms in the heterodevices. Therefore, we investigated the voltage-dependent carrier recombination processes and extracted the ideality factors from the slopes of the *I–V* curves regarding the overall voltage regions. We measured the *I–V* characteristics of the LEDs using a semiconductor parameter analyzer. Figures 1 and 3 present plots of the room-temperature and temperature-dependent *I–V* characteristics, respectively, for the InGaN/GaN MQW LEDs incorporating MQB structures. We extracted the ideality factors from the slopes of the *I–V* curves, which are plotted in Fig. 3 with a log-*I* versus linear-*V* scale. Using Eq. 1, we inferred the corresponding ideality factors from these measurements. The ideality factor (n) had values of 5, 5.15, and 6 at room temperature for the InGaN/GaN MQW LEDs incorporating various In compositions in their MQBs; these values are similar to those described in the literature.[12] The particular current transport mechanisms[10] in nitride-based devices can be characterized in terms of deep-level-assisted tunneling processes arising from the collective effects of the alloy's disorder and the interfacial roughness in InGaN/GaN/metal multijunction structures.

To elucidate the unique correlations existing between the carrier transport and optical characteristics of InGaN/GaN MQW LEDs incorporating MQBs, we examined the radiative recombination of the confined electrons and holes at low temperature. Figure 4 presents the quantum efficiencies of both samples extracted from EL spectra recorded at 20–300 K; the ideality factors ranged from 5 to 80 upon varying the temperature of devices containing the MQBs that had In contents of 0.005, 0.01, and 0.02. We observed a pronounced increase in the ideality factor n, corresponding to a monotonic decrease in the blue emission quantum efficiency, upon decreasing the temperature. The reduction in the EL intensity and

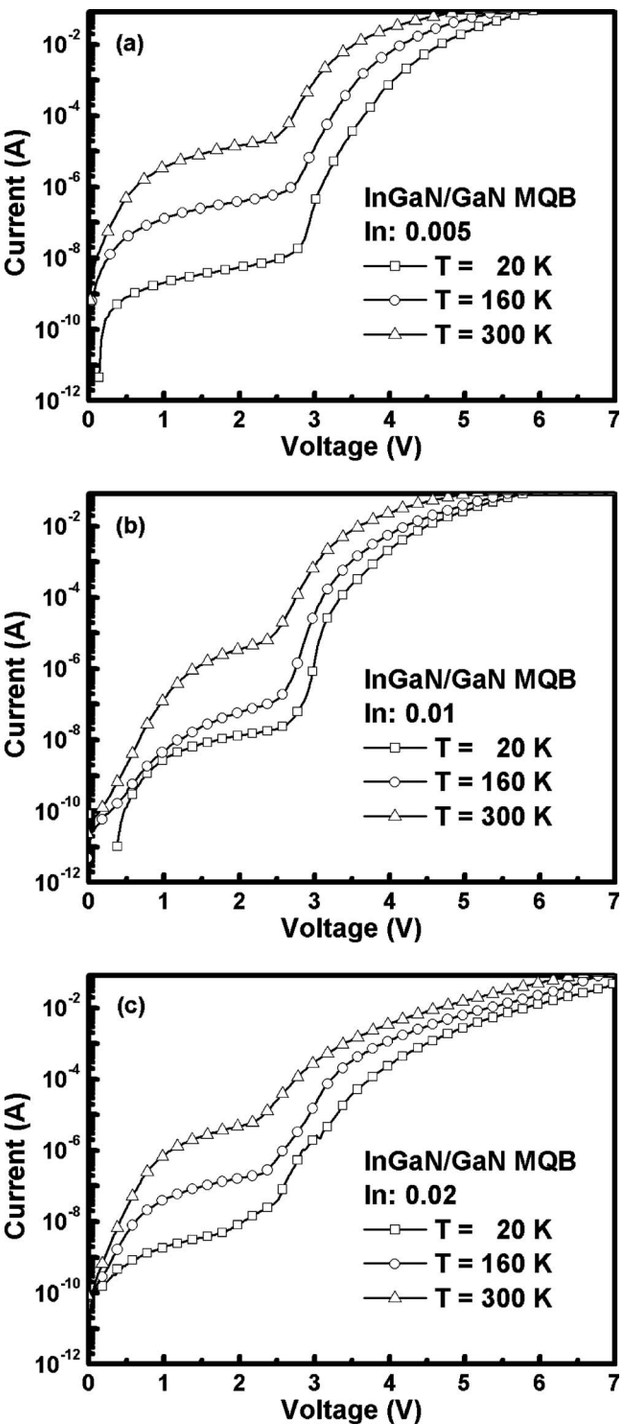

Figure 3. Plots of log I vs V for LEDs incorporating MQBs featuring In contents (x) of (a) 0.005, (b) 0.01, and (c) 0.002, measured at 20 K, 160 K, and room temperature.

quantum efficiency at low temperature was similar to that described previously in a report in which the abnormal behavior manifested the peculiar radiative mechanisms of nitride-based quantum well (QW) heterostructures under electrical excitation.[6] In our present system, the EL intensities and quantum efficiencies of the samples containing various In compositions were all similar within the temperature range from ~180 to 300 K, with the curves almost overlapping each other at 300 K. Therefore, it is not necessarily the case

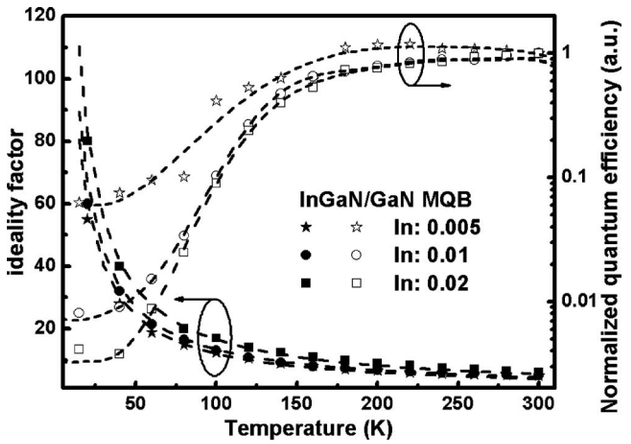

Figure 4. Ideality factor and normalized quantum efficiency plotted with respect to temperature for LEDs incorporating MQBs featuring various In contents.

that a higher content of In provided a higher EL intensity. As the In content decreased, the low rate of change in the spectral intensity, resulting from suppression of the leakage carriers in the MQB structure, led to a high blue spectral efficiency.

From the tunneling current equation proposed by Padovani et al.,[19] we determined the concentrations of interfacial carrier density in the devices from the evolution of the temperature-dependent ideality factor, as follows:

$$n = \frac{q\hbar}{2k_BT}\sqrt{\frac{N_c}{m^*\varepsilon}}\coth\left(\frac{q\hbar}{2k_BT}\sqrt{\frac{N_c}{m^*\varepsilon}}\right) \quad [2]$$

where $\hbar$ is Planck's constant, q is the charge of an electron, k_B is Boltzmann's constant, $m*$ is the effective mass, ε is the dielectric constant, and N_c is the carrier density at the interface of the heterojunction. The calculated ideality factors (dashed lines in Fig. 4) agreed well with our experimental results (dotted lines in Fig. 4), suggesting that the carriers tunneling through the heterojunction were important components in the device. The dashed line in Fig. 4 represents the least-squares fit of Eq. 2 to the experimental data; it agrees quite well with the experimental data. As a result, we determined that the interfacial carrier density in the devices featuring In contents (x) of 0.005, 0.01, and 0.02 in their MQBs was 1.2×10^{18}, 2×10^{18}, and 3.2×10^{18} cm^{-3}, respectively. A higher interfacial carrier density led to a greater number of interfacial states existing in the heterojunction, causing a greater distribution of interfacial states and a less-effective DOS. Moreover, in such heterosystems, the carriers could tunnel through the heterojunction via a greater number of interfacial states to lower the quantum efficiency. Our results also demonstrate that introducing well-designed barriers within a heterojunction configuration can improve device performance by governing the coupling of dynamic transport to spontaneous emissions. Because of a decrease in the DOS, however, the effect on interfacial charge distribution arising from the presence of more charges in the higher-characteristic-energy heterointerfaces reduced the EL intensities of these LEDs considerably at temperatures below 180 K. All observed correlations suggest that the carrier transport process is essentially responsible for the improved luminescence characteristics.

For voltage-dependent carrier recombination processes, the dependence of the ideality factors (extracted from the *I–V* analysis) on temperature and voltage determined the carrier transport mechanisms in the heterodevices. A significant so-called pseudotemperature, T_0, was introduced as a function of the temperature and voltage; it contains information relating to the surface states, determined with respect to the barrier height and Fermi level, according to the unavoidable lattice mismatch in the multiple heterointerfaces. Furthermore, we analyzed the observed leakage current, taking the ideal diode characteristics and recombination current into account in addition to parallel and series resistances. A series resistance can be caused by excessive contact resistance or by the resistance of the neutral regions. A parallel resistance can result from any channel that bypasses the p–n junction; this bypass can be caused by damaged regions of the p–n junction or by surface imperfections. The diode *I–V* characteristics, as given by the Shockley equation, must be modified to take into account parasitic resistance. Assuming a shunt having resistances $R_{parallel}$ (parallel to the diode) and R_{series} (in series with the diode and the shunt), the *I–V* characteristics of a forward-biased p–n junction diode can be represented by

$$I_{junction} = I_s\left\{\exp\left[\frac{e(V - I_{junction}R_{series})}{nkT}\right] - 1\right\} \quad [3]$$

$$\frac{IR_{parallel} - (V - IR_{junction})}{R_{parallel}} = I_{junction} \quad [4]$$

where I_s is the reverse saturation current, e is the electronic charge, k is Boltzmann's constant, T is the thermodynamic temperature, n is the so-called ideal factor of the diode, and I is the total injection current. On the other hand, taking into account the surface-state energy distributions of the interfaces, Levine proposed an alternative approach for measuring the departure of the ideality factor from unity,[13] with a temperature-independent parameter T_0—the so-called pseudotemperature—and the characteristic energy E_0—obtained from *I–V* measurements at various temperatures—used to determine the mechanism of injected current transport. Figure 5 presents plots of the ideality factors with respect to reciprocal temperature over a large range of voltages; the values of the voltage-dependent ideality factors were extracted, using Eq. 3 and 4, from the *I–V* curves in Fig. 3 for devices having In contents (x) of 0.005, 0.01, and 0.02 in their MQBs. Furthermore, using a Levine analysis to provide another description of the configuration of the current flow mechanisms, the dependence of the ideality factors on temperatures is given by[13]

$$n = 1 + \frac{T_0}{T} \quad [5]$$

where T is the measurement temperature in Kelvin and the so-called pseudotemperature T_0 is a temperature-independent parameter associated with the interfacial state distribution at constant current and voltage. Generally, T_0 is a function of temperature (T) and voltage (V); it contains information regarding the surface states. At this point, it is not necessary to give T_0 any further theoretical significance. In principle, T_0 can be determined by measuring the logarithmic slope of the forward-current characteristic for various combinations of T and V. When the bias voltages of the diodes increase, the pseudotemperature T_0 increases accordingly. We found that over a large range of temperatures and voltages, T_0 was independent of the temperature at a constant current and voltage. Furthermore, we found that the low-In-content MQB devices exhibit inherently lower values of T_0 over a variety of temperature ranges. We obtained low values of T_0—associated with a low characteristic energy and a low charge population of the multilayer interface states—for each of our samples in the higher temperature regime. Accordingly, the high-In-content MQB ensemble possessed a relatively higher characteristic energy than that of the low-In-content MQB ensemble. Because an effective DOS is inversely dependent on the above-mentioned characteristic energy E_0, the exciton recombination probability for a large DOS at higher temperature is greater than that for a small DOS at lower temperature. Thus, compared with the high-In-content MQB ensemble, the heterostructure comprising $In_{0.15}Ga_{0.85}N$ wells and $In_{0.005}Ga_{0.995}N$/GaN heterobarriers may intrinsically facilitate an abatement of the interfacial charge distribution, implying a smaller T_0 effect. In contrast, we observed carrier tunneling pro-

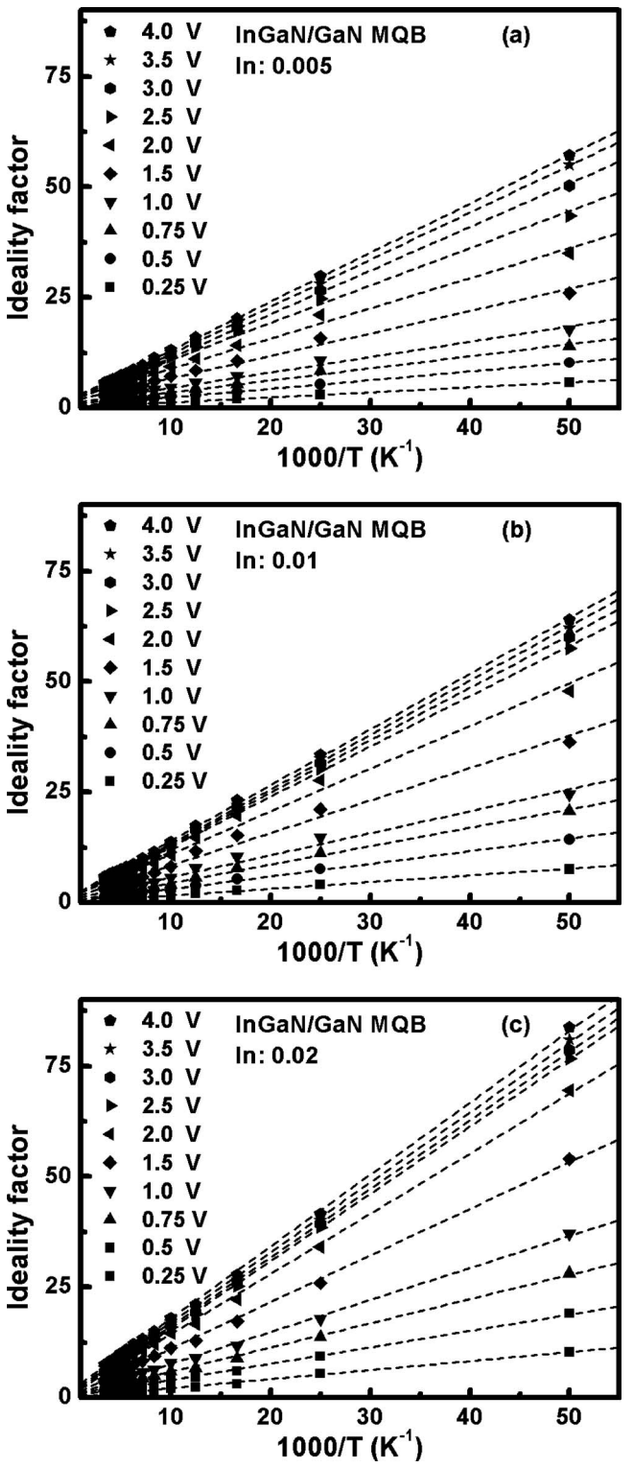

Figure 5. Ideality factor plotted as a function of reciprocal temperature for LEDs incorporating MQBs featuring In contents (x) of (a) 0.005, (b) 0.01, and (c) 0.002.

cesses in terms of the charge population within the high-In-content MQB heterojunctions, which led to a greater T_0 anomaly.

Figure 6 displays the reverse pseudotemperature T_0 plotted with respect to voltage for MQBs having In contents (x) of 0.005, 0.01, and 0.02. We observe that the characteristic energy E_0 of the diodes increased upon increasing the In composition in the $In_xGa_{1-x}N$/GaN

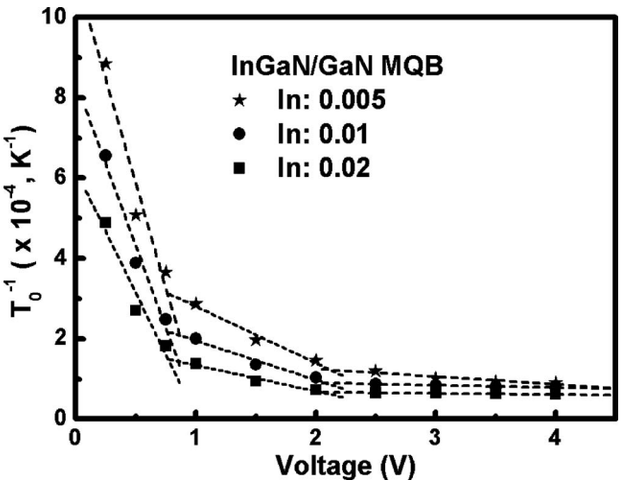

Figure 6. Reverse pseudotemperature T_0 plotted with respect to voltage for LEDs incorporating MQBs featuring In contents (x) of 0.005, 0.01, and 0.02, respectively.

MQBs over each of the three voltage regions: forward bias voltages of less than 1 V (region I), forward bias voltages between 1 and 2 V (region II), and forward bias voltages greater than 2 V (region III). Because the carrier concentration in the depletion region is almost zero, the excess current in region I was due to carrier recombination in the depletion regions through trap levels presumably associated with threading dislocations. In region II, we note that the parallel resistance effectively determined the leakage current; crossover between the leakage current (or recombination current) and diffusion current was strongly affected by the saturation current for the recombination current. Region III can be explained well in terms of the ideal diode equation for p–n junctions, assuming that the diffusion current dominated. Because *I–V* curves suffer from ohmic loss through bulk resistance at high bias voltages, the diode current is basically limited by the series resistance in p-i-n-clad regions. Figure 6 reveals that the characteristic energy E_0 of the diodes increased upon increasing the In composition of the $In_xGa_{1-x}N$/GaN MQBs over each of the three voltage regions. We obtained a low value of T_0 associated with a small characteristic energy and charge population of the multilayer interface states for each sample in the higher temperature regime. Because an effective DOS is inversely dependent on the characteristic energy, the probability of electron/hole recombination for a large DOS at higher voltage is greater than that for a small DOS at lower voltage. Thus, the stronger interfacial state distribution and lower DOS result in the excitons formed in the high-In-content MQB sample deteriorating the spectral radiation over a broad temperature range. Accordingly, the strong T_0 anomaly also leads inherently to rapid thermal quenching of the luminescence in conventional MQW LEDs. Furthermore, for temperatures above 180 K, we found that the excitons formed in the MQB sample augment the spectral radiation due to the decreased interfacial state distribution and greater DOS, as indicated in Fig. 4.

On the other hand, consider the tunneling currents in reverse-biased junctions, expressed using the formula[20]

$$J_r = -V_j C_1 \exp[C_2/(V_{bi} - V_j)^{1/2}] \quad [6]$$

where C_1, C_2, and V_{bi} are constants. The curves in Fig. 7 do not fit the usual model because the current in this model may result from some other mechanism, such as surface leakage or a more complex tunneling mechanism. At more-negative reverse voltages ($V_j < -3$ V), the current is temperature-sensitive and obeys a power law, i.e., $I \propto V^m$. As a result, we suspect that this behavior results from a space-charge-limited current. Not all of the junctions exhibited the temperature-independent region; some displayed more-

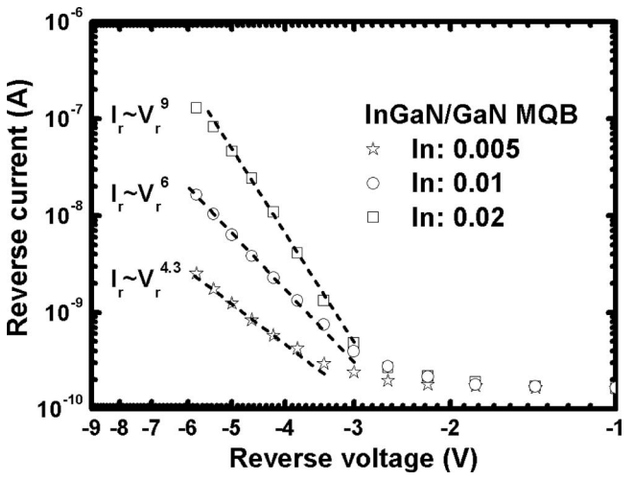

Figure 7. Plots of reverse current vs voltage on a log–log scale for LEDs featuring MQBs containing In contents (x) of 0.005, 0.01, and 0.02, respectively.

conventional I–V characteristics. For the larger junctions, we observed a square-root voltage dependence at low bias, indicative of a space-charge-generated current, and a power-law dependence ($I \propto V^m$) at large reverse bias, again indicating the presence of space-charge-limited currents. The rapid increase in the reverse current at moderate reverse voltages prevented any meaningful determination of the breakdown voltage for these junctions. As the In composition increased, we found that the value of m increased, indicating that the space-charge-limited current dominated the carrier transport mechanism, resulting in augmentation of the ideality factor and reduction of the luminescence efficiency of the InGaN/GaN MQW LEDs incorporating MQBs.

Conclusion

Over a broad range of temperatures, unique correlations exist between the electrical characteristics and optical properties of InGaN/GaN MQW LEDs incorporating MQBs. From the L–I–V characteristics of InGaN/GaN MQW LEDs, we observed a remarkable reduction and modulation in the distribution of leakage charges, resulting in the inhibition of nonradiative recombination and the enhancement of localization effects when adopting the MQB structure. Based on I–V analyses, these observed correlations suggest that the carrier transport process is essentially responsible for the improvement in the luminescence characteristics. It appears that there is an essential link between the material quality and the mechanism of current transport through the wide-bandgap p-i-n junction. Temperature-dependent EL spectra revealed that devices incorporating MQB structures exhibited higher emission intensities and were less sensitive to temperature. These results suggest the inhibition of carrier nonradiative recombination and the enhancement of exciton localization effects. The In content affected the light output intensity of the LEDs. As the In content decreased, a low rate of decrease in intensity, resulting from suppression of the leakage carriers in the MQB structure, led to a high blue spectral efficiency; lower values of the pseudotemperature T_0 and the characteristic energy E_0, resulting from the augmented spectral radiations at temperatures above 180 K, were due to the decreased interfacial state distribution and greater DOS. We associated this behavior with a low characteristic energy and a low charge population of the multilayer interface states for each sample in the higher temperature regime. Correspondingly, from EL spectra measured over a broad temperature range, we found that the spectral intensity deteriorated, resulting in low charge populations in the multilayer interfacial states and a more-effective DOS. These observed correlations suggest that the carrier transport process was essentially responsible for the improvements in the luminescence characteristics.

Acknowledgments

We thank the staff of the Group of Abel and Lie Operations In Sciences and Quantum Electro-optical Science and Technology Laboratory (GALOIS-Quest-Lab), Department of Electronic Engineering, Chang Gung University, Taiwan, for support. This study was supported by the National Science Council of Taiwan under Contract no. NSC 97-2112-M-182-002-MY3.

Chang Gung University assisted in meeting the publication costs of this article.

References

1. I. Akasaki and H. Amano, *Jpn. J. Appl. Phys., Part 1*, **36**, 5393 (1997).
2. S. Nakamura, M. Senoh, S. Nagahama, N. Iwasa, T. Yamada, T. Matsushita, H. Hiyoku, Y. Sugimoto, T. Kozaki, H. Umemoto et al., *Jpn. J. Appl. Phys., Part 2*, **36**, L1568 (1997).
3. I. Schnitzer, E. Yablonovitch, C. Caneau, T. J. Gmitter, and A. Scherer, *Appl. Phys. Lett.*, **63**, 2174 (1993).
4. S. F. Chichibu, M. Sugiyama, T. Onuma, T. Kitamura, H. Nakanishi, T. Kuroda, A. Tackeuchi, T. Sota, Y. Ishida, and H. Okumura, *Appl. Phys. Lett.*, **79**, 4319 (2001).
5. C.-K. Sun, S. Keller, G. Wang, M. S. Minsky, J. E. Bowers, and S. P. DenBaars, *Appl. Phys. Lett.*, **69**, 1936 (1996).
6. R. M. Lin, C. H. Lin, J. C. Wang, T. E. Nee, B. R. Fang, and R. Y. Wang, *J. Cryst. Growth*, **278**, 421 (2005).
7. C. M. Lee, C. C. Chuo, K. F. Dai, X. F. Zheng, and J. I. Chyi, *J. Appl. Phys.*, **89**, 6554 (2001).
8. M. A. Reshchikov, G.-C. Yi, and B. W. Wessels, *Phys. Rev. B*, **59**, 13176 (1999).
9. K. Iga, H. Uenohara, and F. Koyama, *Electron. Lett.*, **22**, 1008 (1986).
10. R. M. Lin, J. C. Wang, C. H. Lin, T. E. Nee, C. A. Huang, B. R. Fang, and R. Y. Wang, *J. Vac. Sci. Technol. B*, **23**, 966 (2005).
11. T. E. Nee, H. T. Shen, J. C. Wang, and Y. F. Wu, *J. Appl. Phys.*, **101**, 023703 (2007).
12. J. M. Shah, Y.-L. Li, Th. Gessmann, and E. F. Schubert, *J. Appl. Phys.*, **94**, 2627 (2003).
13. J. D. Levine, *J. Appl. Phys.*, **42**, 3991 (1971).
14. T. E. Nee, H. T. Shen, J. C. Wang, and R. M. Lin, *J. Cryst. Growth*, **287**, 468 (2006).
15. X. A. Cao, E. B. Stokes, P. Sandvik, S. F. Leboeuf, J. Kretchmer, and D. Walker, *IEEE Electron Device Lett.*, **23**, 535 (2002).
16. E. S. Yang, C. M. Wu, and R. Y. Hung, *J. Appl. Phys.*, **51**, 1262 (1980).
17. D. Zhu, J. Xu, A. N. Noemaun, J. K. Kim, E. F. Schubert, M. H. Crawford, and D. D. Koleske, *Appl. Phys. Lett.*, **94**, 081113 (2009).
18. C. Sah, R. N. Noyce, and W. Shockley, *Proc. IRE*, **45**, 1228 (1957).
19. F. A. Padovani and R. Stratton, *Solid-State Electron.*, **9**, 695 (1966).
20. A. R. Riben and D. L. Feucht, *Solid-State Electron.*, **9**, 1055 (1966).